JACS
JOURNAL OF THE AMERICAN CHEMICAL SOCIETY

Article

pubs.acs.org/JACS

Carbohydrate Affinity for the Glucose–Galactose Binding Protein Is Regulated by Allosteric Domain Motions

Gabriel Ortega, David Castaño, Tammo Diercks, and Oscar Millet*

Structural Biology Unit, CIC bioGUNE, Bizkaia Technology Park, Building 800, 48160 Derio, Spain

Supporting Information

ABSTRACT: Protein function, structure, and dynamics are intricately correlated, but studies on structure–activity relationships are still only rarely complemented by a detailed analysis of dynamics related to function (functional dynamics). Here, we have applied NMR to investigate the functional dynamics in two homologous periplasmic sugar binding proteins with bidomain composition: *Escherichia coli* glucose/galactose (GGBP) and ribose (RBP) binding proteins. In contrast to their structural and functional similarity, we observe a remarkable difference in functional dynamics: For RBP, the absence of segmental motions allows only for isolated structural adaptations upon carbohydrate binding in line with an *induced fit* mechanism; on the other hand, GGBP shows extensive segmental mobility in both *apo* and *holo* states, enabling selection of the most favorable conformation upon carbohydrate binding in line with a *population shift* mechanism. Collective segmental motions are controlled by the hinge composition: by swapping two identified key residues between RBP and GGBP we also interchange their segmental hinge mobility, and the doubly mutated GGBP* no longer experiences changes in conformational entropy upon ligand binding while the complementary RBP* shows the segmental dynamics observed in wild-type GGBP. Most importantly, the segmental interdomain dynamics always increase the apparent substrate affinity and thus, are functional, underscoring the allosteric control that the hinge region exerts on ligand binding.

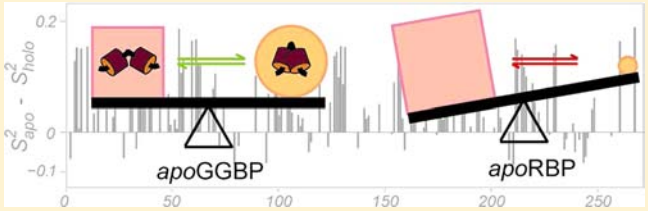

INTRODUCTION

Complex protein motions become functionally relevant when the number of implicated residues increases (cf. functional dynamics),[1] and ligand-induced rearrangements comprising entire domains or large protein segments are frequently found in subcellular processes like signal gating, regulation, substrate uptake, and enzyme catalysis.[2−4] The structural determinants for such concerted dynamics are therefore of key interest. While structural data are often available for many instants in the trajectory,[5] this alone cannot unequivocally identify the minimal set of amino acids responsible for the conformational transitions, which ultimately is the information required for understanding and mastering the motional event.

Periplasmic binding proteins (PBPs) constitute a large family of receptors that recognize a plethora of small molecules and ions in Gram-negative bacteria.[6] Through substrate binding, PBPs serve as intermediary receptors in the ABC transport system[7] and trigger bacterial chemotaxis.[8] PBPs represent a paradigm for functional dynamics: binding is associated with a large closure motion that traps the ligand in the cleft between both protein domains,[9,10] and this "Venus flytrap" mechanism is also employed by many human receptors.[11,12] The very high substrate affinity has been exploited for the design of nanosensors that, based on the changes in molecular properties associated with the closure event, are able to detect down to nanomolar concentrations of metabolites and ions.[13,14] In the absence of a ligand, the molecule is expected to stay in the open state, but excursions to more closed conformations have been demonstrated for the *apo* protein by molecular dynamics (MD) simulations,[15,16] NMR spectroscopy,[17,18] and X-ray crystallography.[19] In many cases, structural data and computational studies have provided clear descriptions for the conformational trajectory[20,21] and have identified the residue composition in the hinge region as a crucial element for the closure mechanism.[22,23] Still, the nature and time scales for the collective dynamics remain elusive.

Here we present a detailed study of two structurally homologous PBPs: *Escherichia coli* ribose binding protein (RBP) and glucose/galactose binding protein (GGBP). Our NMR studies show that free RBP in solution adopts a domain orientation that largely agrees with published X-ray data for the crystalline state. NMR relaxation data for *apo*- and *holo*RBP confirm a canonical closure mechanism during ligand uptake. For GGBP, no single structure can satisfy the experimental NMR data, and increased backbone dynamics is widely observed in the ligand-bound form. We furthermore demonstrate that the domain motions detected in GGBP are cooperative and exclusively governed by the hinge composition. Although the hinge region is far away from the monosaccharide binding site, it alters the protein's affinity for the sugar, underscoring the intimate relationship between domain reorientation and the binding free energy.

Received: September 19, 2012
Published: November 14, 2012

   dx.doi.org/10.1021/ja3092938 | J. Am. Chem. Soc. 2012, 134, 19869–19876

EXPERIMENTAL SECTION

Sample Preparation and Chemical Shift Assignment. The *E. coli* protein genes for RBP and GGBP (encoding for 271 and 309 amino acids, respectively, without the signal peptidase sequence) were amplified by PCR reaction and subsequently subcloned into a pET11d overexpression destination vector (New England Biolabs) using the *Bam*HI and *Nco*I restriction sites. Uniformly labeled (^{15}N, ^{13}C, ^{2}H) RBP and GGBP proteins were overexpressed in deuterated M9 media (1.5 L, purchased from CIL) containing $^{15}NH_4Cl$, ^{13}C-glucose, and D_2O as the only sources for nitrogen, carbon, and deuterium, respectively. High levels of deuteration (>85% on average) were achieved in both cases. Proteins were purified via ion exchange chromatography using fast flow Q-Sepharose followed by ion exclusion cromatography (Superdex 75, GE Healthcare) in 20 mM Tris buffer at pH 7.1, 150 mM NaCl. To eliminate bound sugars, the proteins were dialyzed several times against 3.5 M guanidinium chloride under same buffer conditions. Final sample conditions: 1.0 mM RBP or GGBP in 20 mM Tris, 150 mM NaCl, 10 mM $CaCl_2$, 95%/5% H_2O/D_2O, pH 7.0, and 3 mM D-glucose (optional).

All experiments were carried out at 310K on a Bruker Avance III 800 MHz spectrometer equipped with a TCI cryoprobe, on a Bruker Avance III 600 MHz spectrometer, or on a Varian Innova 500 MHz spectrometer. The NMR data were processed using NMRPipe and analyzed with NMRView.[24] Assignment of backbone resonances for *apo*RBP, *apo*GGBP, *glu*RBP, and *glu*GGBP relied on the following 3D spectra (all TROSY versions): HNCO, HNCA, HN(CO)CA, HNCB, and HN(CO)CB (both with constant t(CB) time = 26 ms for CBC_n multiplicity encoding), as described previously.[25] The backbone assignments for the four proteins have been deposited in the Biological Magnetic Resonance Data Bank (BioMagResBank, http://www.bmrb.wisc.edu) under the accession codes 18597 (*apo*RBP), 18601 (*apo*GGBP), 18603 (*glu*RBP), and 18609 (*glu*GGBP). Nearly complete assignments for the non-proline backbone resonances ($^{13}C\alpha$, $^{13}C\beta^{13}C'$, ^{1}HN, and ^{15}N) were achieved: 95% (*apo*RBP), 94% (*apo*GGBP), 95% (*gluRBP*), and 86% (*glu*GGBP). The assignments (^{1}H and ^{15}N for *apo*- and ligand bound forms) for the two double mutants considered in the present work (A102G/S103T-RBP and G109A/T110S-GGBP) were achieved by comparison with their respective wild types ^{1}H,^{15}N-HSQC and verification in a 3D ^{1}H,^{15}N-HSQC-NOESY spectrum.

Measurement of Residual Dipolar Couplings and Solution Structure Elucidation. The proteins were aligned in 1,2-dihexanoyl-*sn*-glycero-3-phosphocholine (DHPC) and 1,2-dimyristoyl-*sn*-glycero-3-phosphocholine (DMPC) bicelles (2.8:1 molar ratio, Avanti Lipids). The final concentration of total lipid was 0.03 g/mL, leading to a residual ^{2}H water splitting of 8−12 Hz. ^{1}H,^{15}N dipolar couplings ($^{1}D_{HN}$) were measured using a regular 3D HNCO (TROSY) experiment, a *J*-scaled (α = 1) 3D HNCO (TROSY) experiment,[26] and edited ^{1}H,^{15}N-HSQC experiments.

Dipolar couplings were used to determine the interdomain orientation for GGBP and RBP (in both *apo* and *holo* forms), following the protocol described by Evenas et al.[27] The X-ray structures from open and closed forms of *E.coli* GGBP (2GBP,[10] 2HPH,[28] 2FW0[23]) and *E.coli* RBP (1URP[29] and 2DRI[30]) were employed as models to derive the solution structure of the proteins. An algorithm implemented within the CNS software package[31] uses the experimental set of residual dipolar couplings (RDCs) as the only experimental restraints to reorient the domains.[17] RDCs from residues belonging to flexible regions (according to relaxation data) were not included in the analysis, and a total of 172 and 160 $^{1}D_{HN}$ values were used for *apo*RBP and *apo*GGBP, respectively. Synthetic intradomain restraints (N−N and H^N−H^N distances, and ϕ and ψ backbone dihedral angles) were generated for each protein to ensure that the individual domain structures remained invariant during the minimization procedure.[20] The final structures are the averages of 12*n* solution conformations, where *n* is the number of starting structures employed.

Relaxation Measurements and Model-Free Analysis. Backbone amide relaxation data (^{15}N R_1, R_2 and ^{15}N{^{1}H} heteronuclear NOE) were measured at two magnetic fields (600 MHz and 800 MHz) for *apo*GGBP and for *apo*RBP additionally at 500 MHz. The pulse sequences reported by Farrow et al.[32] were employed. The temperature was calibrated by measuring the residual signal separation in a 99.8% D_4-methanol reference sample. Typically, between 10 and 12 time points were recorded for each relaxation rate (R_1 or R_2) in interleaved mode and including at least two duplicate points to estimate the error. Relaxation delays ranged between 10 ms and 1.2 s for R_1, and between 10 ms and 120 ms for R_2. In the R_2 experiment, compensatory CMPG pulsing before the interscan recovery delay corrected for the different sample heating from CPMG pulsing during the actual scan. For the heteronuclear NOE experiment, steady-state H^N saturation was achieved with a 4 s train of 120° pulses, and a 12 s interscan delay was used in the reference spectrum to ensure full reequilibration.

The R_1 and R_2 data sets recorded at the highest magnetic field (800 MHz) were used to derive the rotational diffusion tensor. Residues exhibiting large amplitude motions on the picosecond-to-nanosecond time scale (recognized by small, or negative ^{15}N{^{1}H} NOE) were excluded from the diffusion tensor calculations. First, each residue's R_2/R_1 ratio was converted into a local diffusion constant ($D_i = 6\tau_i^{-1}$) using our own scripts. Subsequently, all local diffusion constants were simultaneously fit to a structural model using the *quadric* program (Prof. Palmer, Columbia University, http://www.palmer.hs.columbia.edu/software/quadric.html) to determine fully anisotropic, axially symmetric, and isotropic diffusion tensors.[33,34] The fitting error (χ^2_{red}) corresponds to the difference between experimental and calculated values (χ^2) divided by the number of data points (n). The structural models tested included *apo*RBP (1URP),[29] *apo*GGBP (2FW0),[23] *glu*RBP (2DRI),[30] and *glu*GGBP (2HPH, 2GBP)[10,28] as well as our NMR solution structures for RBP and GGBP (present work). Based on F-tests we then selected either the fully anisotropic, axially symmetric, or isotropic rotational diffusion tensor. Relaxation data were used to estimate the average interdomain orientation in solution following the above-mentioned protocol. A set of structures with varying hinge angles were fitted to the relaxation data sets, and F-test statistics was used to determine the uncertainty in the interdomain orientation.

The backbone ^{15}N relaxation data were also analyzed in terms of the Lipari−Szabo formalism[35] using own scripts. For a given protein, all available relaxation data were simultaneously fit to three different model-free functions: LS-2 with a generalized order parameter (S^2) and local correlation time for picosecond motions (τ_e), LS-3 that assumes a local rather than molecular correlation time (τ_i),[36] and LS-4 that includes a specific order parameter (S_f^2) and correlation time (τ_f) for intermediate local motions. Considering the large number of experimental ^{15}N relaxation data available, the models were recalculated using only a subset of the data to check for consistency. In all calculations, the ^{15}N chemical shift anisotropy was set to −170 ppm and the effective N−H bond length to 1.02 Å. Errors were derived from the experimental uncertainties by Monte Carlo analysis. Chemical exchange contributions in the measured ^{15}N R_2 rates could be excluded on the basis of relaxation dispersion experiments performed for *apo*RBP, *apo*GGBP, *glu*RBP, and *glu*GGBP (data not shown).

The changes in conformational entropy associated with changes in generalized order parameters (obtained via function LS-2) were determined using the relationship described by Yang and Kay.[37] The uncertainty in calculated entropy was determined by standard error propagation from the uncertainty in the fitted function.

Isothermal Titration Calorimetry. Affinity constants for D-glucose were determined at 310 K by isothermal titration calorimetry using a VP-ITC calorimeter (Microcal). Protein concentrations of 60 μM and 200 μM were used for (wt and mutant) GGBP and RBP, respectively, in a final sample volume of 1.8 mL. The reference cell (same volume) was filled with the protein buffer: 20 mM Tris, 150 mM NaCl, 10 μM $CaCl_2$, pH 7.0. The experiment used an initial delay of 60 s and was divided into 30 injections of 5 μL (GGBP) or 10 μL (RBP) aliquots of the titrant (2 mM D-glucose and 1 mM D-ribose).

dx.doi.org/10.1021/ja3092938 | J. Am. Chem. Soc. 2012, 134, 19869−19876

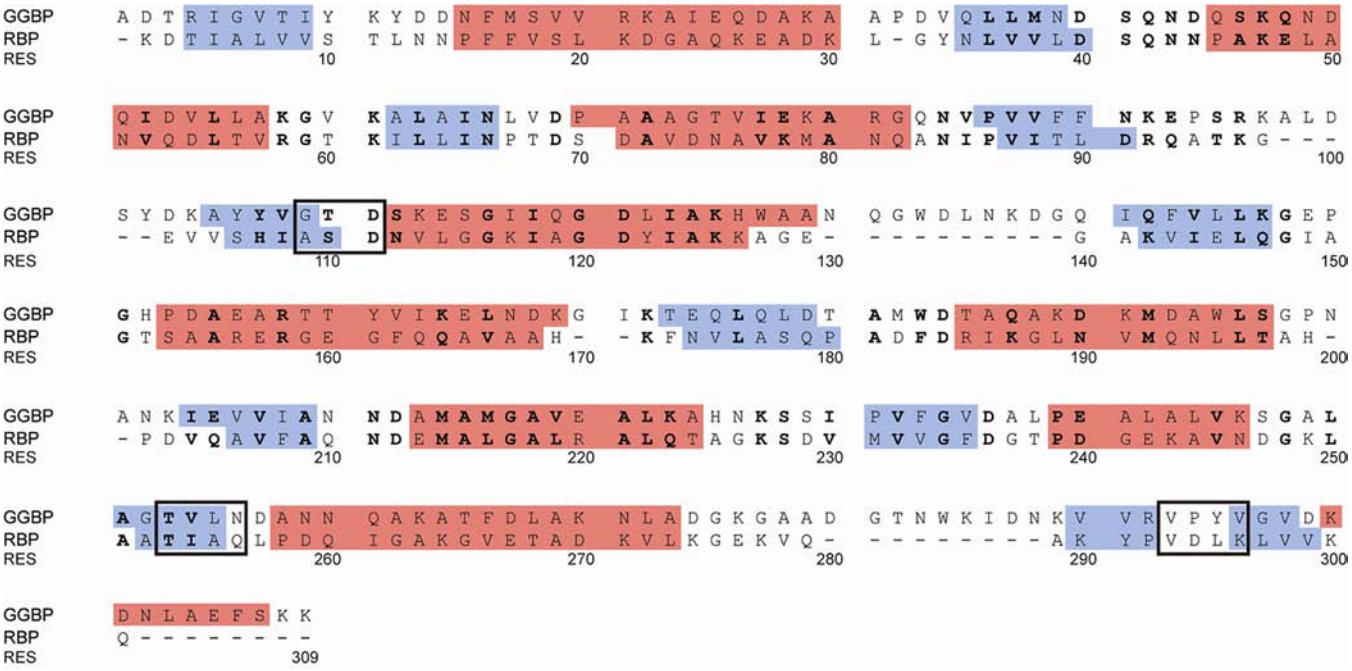

Figure 1. Sequence alignment and secondary structure comparison for *E. coli* GGBP and *E. coli* RBP. Identical residues between the two proteins are bold highlighted. Red and blue residues correspond to α-helical and β-sheet regions, respectively, while hinge elements are located with black squares.

The data were analyzed with the program Origin, integrated in the calorimeter software.

RESULTS

Domain Orientation in Solution for GGBP and RBP. *E. coli* GGBP (33.4 kDa) and *E. coli* RBP (28.5 kDa) exhibit only 24% sequence identity (Figure 1), but a very high homology in their structures[38] that are composed of two globular domains with Rossman fold and similar size, connected by a hinge region composed of three β-strands.[9,39] The natural substrates for GGBP and RBP are D-galactose and D-ribose, respectively, but both proteins also bind D-glucose with moderate to high affinity.[40] X-ray structures from different organisms show that their *apo* states (*apo*RBP and *apo*GGBP) can adopt different domain orientations.[23,29] Such conformational heterogeneity may be due to intrinsic mobility, or a crystallization artifact. Structural data for *apo*GGBP and *apo*RBP reporting on their domain orientation in solution are therefore desirable and can be obtained by NMR spectroscopy. Both proteins show excellent signal dispersion in their $^{1}H,^{15}N$-HSQC spectrum (Figures S1 and S2), and conventional triple-resonance experiments yielded nearly complete backbone assignments. RDCs that report on the average molecular orientation within an alignment medium (i.e., a diluted liquid crystalline solution)[41] were used as experimental restraints to derive the backbone structures for *apo*RBP and *apo*GGBP. The protocol was identical for both proteins: residual $^{1}D_{HN}$ couplings were measured for 172 (*apo*RBP) and 160 (*apo*GGBP) backbone amide groups within the structured regions and used to refine each domain structure independently. Then, the domains were treated as rigid bodies, while the experimental RDC data were used as restraints in a simulated annealing protocol to define the domain orientation.

The derived NMR solution structures for *apo*RBP and *apo*GGBP are shown in Figure 2A. To describe the relative domain orientation, each structure was analyzed in terms of a hinge (θ) and a twist (ϕ) angle (Table S1). This is a convenient way of expressing the absolute interdomain orientation for a PBP since θ experiences large changes during ligand uptake.[42] For *E. coli apo*RBP, our NMR solution structure has a hinge angle (127°) that agrees very well with both the X-ray crystal structure (1URP, 130°)[29] and the minimal free energy conformation (129°) obtained from MD simulations.[42] For GGBP, analysis of all available structure data reveals a manifold of hinge angles (Table S1) ranging from 124° to 149° for *apo*GGBP, and from 120° to 124° for *holo*GGBP. Interestingly, the NMR solution structure for *apo*GGBP presents an intermediate conformation that is structurally more related to the ligand-bound *holo* conformations, or to the *S. typhimurium apo*GGBP structure.[19] The hinge angle dispersion suggests high protein flexibility in solution, where a major (semiclosed) conformation would experience excursions toward transient open conformations. To verify this hypothesis, backbone relaxation measurements were carried out.

Fast Protein Motions Persist after Carbohydrate Binding. NMR relaxation data provide information about the rotational diffusion of the molecule (with correlation time τ_c), and superimposed faster local or segmental motions.[43] For each protein, ^{15}N relaxation data (T_1, T_2, and $^{15}N\{^{1}H\}$-NOE) were measured for the backbone amide groups (212 and 204 residues in *apo*RBP and *apo*GGBP, respectively) at three magnetic fields (500, 600, and 800 MHz). The rotational correlation time τ_c can be derived from the T_1/T_2 distribution,[44] but the analysis is much more accurate when structural data are included to model the rotational diffusion anisotropy.[33,34] Our statistical F-test analysis confirmed an axially symmetric molecular rotation tensor (with overall correlation time τ_c and anisotropy factor D_{par}/D_{per} as listed in Table S2). For *apo*RBP, the NMR structure yielded better anisotropy fitting for the relaxation data than the *E. coli* X-ray structures with open (1URP)[29] or closed (2DRI)[30] domain

dx.doi.org/10.1021/ja3092938 | J. Am. Chem. Soc. 2012, 134, 19869−19876

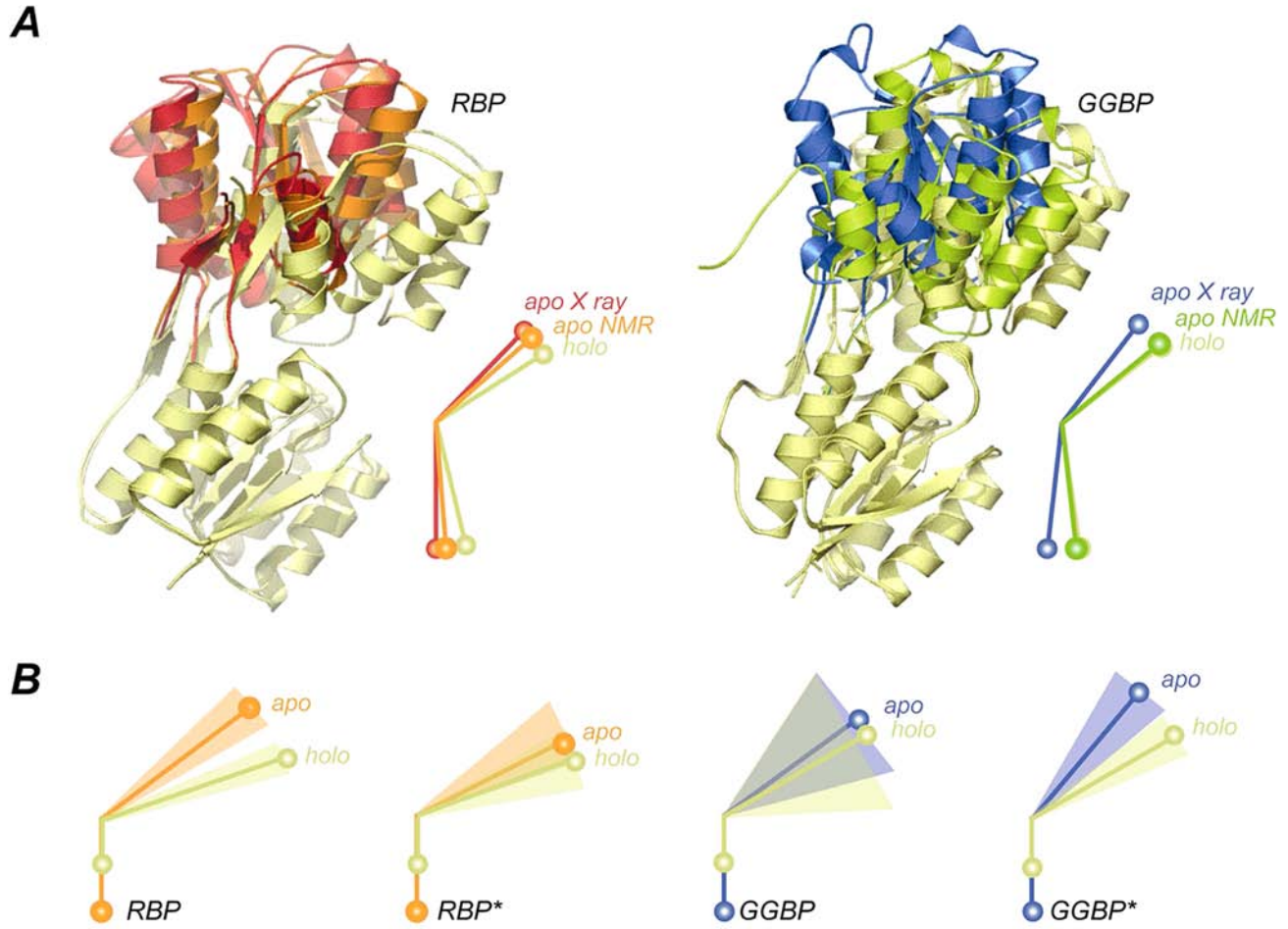

Figure 2. (A) Overlay of the different *E. coli* RBP and GGBP structures, aligned by the N-domain: solution NMR conformation (orange/green) and crystalline structures for the *apo* (red/blue) and *holo* (yellow) states. The inset model represents the domains as balls and sticks to reproduce the interdomain hinge angles (θ) for the above-mentioned states. (B) Identical schematic representation to now show the interdomain angles obtained from the rotational diffusion tensor analysis. The shade areas reflect the uncertainty in the angle determination, according to F-test statistics.

orientations. When both domains were analyzed separately (to evince the contribution from domain reorientation), the resulting tensors were very similar to the one obtained for the whole *apo*RBP, indicating that, within experimental error, a single conformation (i.e., the NMR solution structure) satisfies all experimental constraints (Figure 2B). Nevertheless, domain dynamics in *apo*RBP cannot be ruled out completely since motions with a frequency $\omega \ll (\tau_c)^{-1}$ would not significantly affect the relaxation of the nuclear spin. The excellent agreement found for *apo*RBP again contrasts with *apo*GGBP where no single structure can satisfy the relaxation data (resulting in high χ^2_{red} deviations, Figure 2B). Moreover, our analysis for the individual domains yielded slightly different domain correlation times (and lower χ^2_{red} values, Table S2) as indirect evidence for domain motions in *apo*GGBP.

We also measured ^{15}N relaxation data (T_1, T_2, and ^{15}N{^{1}H}-NOE) at two different fields (600 and 800 MHz) for both proteins in their *holo* form bound to glucose (*glu*GGBP and *glu*RBP). The ^{1}H,^{15}N-HSQC spectra for *glu*GGBP and *glu*RBP (Figures S3 and S4) differ significantly from those of their *apo* forms and had to be reassigned. The rotational diffusion tensors for the *holo* proteins were derived from the experimental relaxation data sets (Figure 2B and Table S3). Moreover, *apo* and ligand-bound *holo* form ^{15}N relaxation data were analyzed using the Lipari–Szabo *model-free* formalism (Table S4) that makes no assumptions on the motional mechanism (but on the number of uncorrelated superposed modes) and only requires the fast local librations to be uncorrelated with the overall tumbling of the molecule.[35] The simplest considered model-free function (LS-2) yields an order parameter S^2 that gauges the amplitude of a local angular motion of an amide H–N vector and its effective correlation time τ'. In all cases, large S^2 were found, characteristic for the backbone of a compactly folded, globular protein (Figure S5). Figure 3 shows the changes in S^2 upon ligand binding ($\Delta S^2 = S^2_{apo}S^2_{holo}$) for both proteins. For RBP, ΔS^2 oscillates between positive and negative values without a clear trend. For GGBP, however, the vast majority of residues in GGBP present positive ΔS^2 values that result in a net positive contribution and indicate a widespread increase of flexibility for *glu*GGBP relative to *apo*GGBP.

This observation is intriguing, but not unprecedented since several earlier studies have revealed widespread changes in pico- to nanosecond protein backbone dynamics upon ligand binding,[45,46] including several cases of protein–carbohydrate interactions[47] and at least one study on a PBP.[48] In principle, this effect can be attributed to increased fast librations of the amide bonds in *glu*GGBP to compensate for the restricted motional freedom of the domains upon ligand binding. Alternatively, the discrepancy may be caused by concerted segment motions on a slower time scale close to τ_c that affect

dx.doi.org/10.1021/ja3092938 | J. Am. Chem. Soc. 2012, 134, 19869–19876

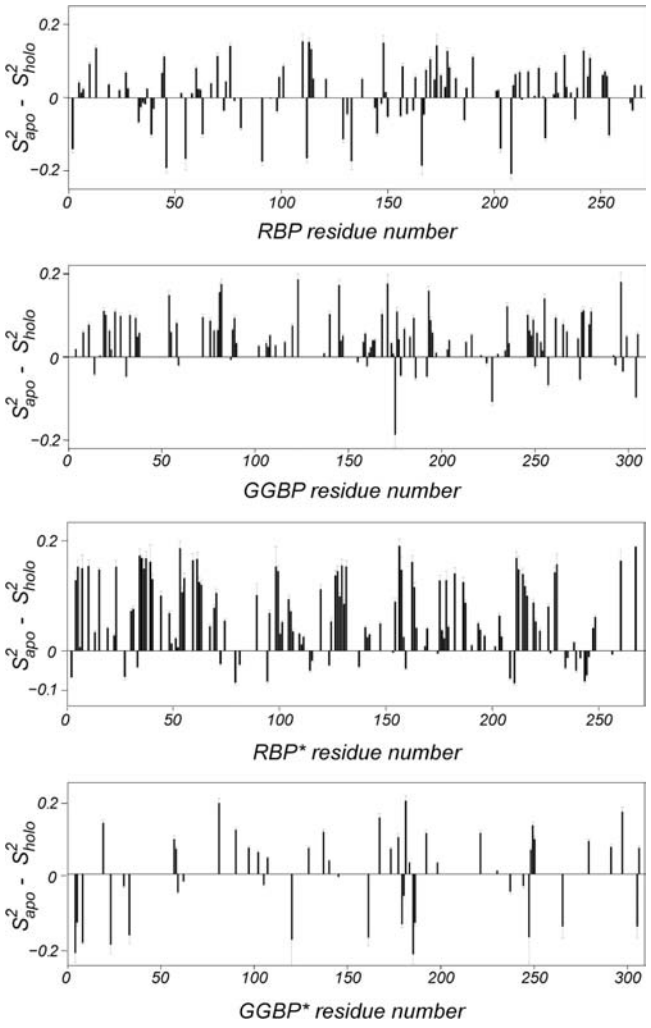

Figure 3. Changes in generalized order parameters $\Delta S^2 = S^2_{apo} - S^2_{holo}$ as a function of the residue number for all four proteins considered in the study (as indicated in the abscise axes). Error bars correspond to propagated uncertainties in the relaxation rates derived by Monte Carlo analysis.

the order parameters and violate the required temporal separation between local and overall motions. To investigate this possibility, S^2 values for the four data sets (*apo*RBP, *glu*RBP, *apo*GGBP, and *glu*GGBP) were also obtained from a modified model-free function (LS-3, Table S4) where the overall rotation correlation time τ_c is replaced by individual effective correlation times for each residue, τ_i[36] (Figure S6). For *apo*RBP, *glu*RBP, and *apo*GGBP both functions yield equivalent results: the distribution of τ_i is centered around τ_c and the S^2 obtained by fitting to functions LS-2 and LS-3 agree well. For *glu*GGBP the S^2 values are slightly, but systematically, higher when fitting to the extended function LS-3, suggesting that segmental nanosecond dynamics may also contribute to the order parameter. Analysis with a more complex model-free function that additionally resolves a second-order parameter for slow local motions[49] (LS-4, Table S4) yielded equivalent results (data not shown). The identified segmental nanosecond motions can explain the multiple hinge angles θ (with divergence up to 9°) observed in the set of available *holo*GGPB structures.[23]

The order parameter S^2 derived from model-free analysis of NMR relaxation data is related to the conformational entropy **S**, as demonstrated by Yang and Kay.[50] With the available data (108 residues for GGBP and 107 residues for RBP), average changes in conformational entropy upon ligand binding,

$$\overline{\Delta \mathbf{S}_i} = \overline{\mathbf{S}_i(apo) - \mathbf{S}_i(holo)}$$

were calculated for both proteins (Figure S7). RBP shows a negligible change in conformational entropy (-0.3 ± 0.1 J·mol^{-1}·K^{-1}), as expected from the lack of any trend in the ΔS^2 changes of order parameters. For GGBP, the net entropy change $\overline{\Delta \mathbf{S}_i}$ associated with the observed change in local (pico- to nanosecond) dynamics amounts to -2.4 ± 0.4 J·mol^{-1}·K^{-1} and contributes to stabilizing the protein−sugar complex. Although this approximate value for $\overline{\Delta \mathbf{S}_i}$ is limited by the incomplete data available and possibly overestimated due to some bias in the order parameters S^2 (LS-2) from nanosecond motions in *glu*GGBP, the overall increase in conformational entropy upon binding is evident (cf. Figure 3). A very similar entropic contribution found for the structurally homologous arabinose binding protein[48] corroborates the idea that this stabilizing mechanism is common among carbohydrate binding proteins.

Fast Dynamics Are Correlated and Governed by the Hinge. An important question is whether the motions identified in *glu*RBP only reflect uncorrelated thermal motions, or are of a much more complex and concerted nature. Provided that the motions are correlated and can be described as transitions between protein conformations where the domains act as rigid bodies, their structural determinant must lie in the hinge region connecting both domains. To test this hypothesis, we mutated residues in the hinge region of both proteins. Their common hinge topology comprises three β-strands with only 18% sequence conservation (Figure 1) and relative rigidity due to steric obstruction through bulky side chains. Based on changes in their backbone dihedral angles (ϕ and ψ) between *apo*GGBP and *glu*GGBP, amino acids G109 and T110 (to minor extent also Y111 and V293) were identified as key residues for the interdomain dynamics (Figure S8). For RBP, torsion angle changes were most pronounced for residues A102, V263, and K266. According to sequence alignment, V293 in GGBP and V263 in RBP occupy equivalent positions, while K266 (RBP) is very close to the protein's C-terminus and therefore not considered further. Our analysis is consistent with a previous calculation of backbone dihedral angles for GGBP and RBP[23] showing that the conformational changes between open and closed conformations, and differences in these changes between both proteins, are most pronounced in the first β-strand of the hinge (residues 109−111 in GGBP and 102−104 in RBP). Based on these considerations, two modified proteins were engineered by site-directed mutagenesis: (i) G109A/T110S-GGBP (GGBP*) that exchanges the two critical GGBP residues for their RBP counterparts in the first strand of the hinge, and (ii) the counterpart double substitution A102G/S103T-RBP in RBP (RBP*).

NMR spectra of the mutant proteins are very similar to the wild type (wt), indicating their congruent fold. In addition, the double hinge residue mutations do not significantly alter the proteins' stability, according to thermal denaturing experiments (data not shown). ^{1}H,^{15}N-HSQC-NOESY experiments on the [U-^{15}N]-labeled mutant proteins were sufficient to derive their backbone amide (^{1}H and ^{15}N) assignments in both *apo* and *holo* forms), based on the wt assignments. Furthermore, ^{15}N relaxation data (T_1, T_2, and ^{15}N{^{1}H}-NOE) were collected at two different magnetic fields (600 and 800 MHz) for both

dx.doi.org/10.1021/ja3092938 | J. Am. Chem. Soc. 2012, 134, 19869−19876

Table 1. Affinity for the Natural Ligand, As Measured by Isothermal Titration Calorimetry

	wild-type			mutant		
protein	K_D/nM	$\Delta H°$/kcal·mol^{-1}	$T\Delta S°$/kcal·mol^{-1}	K_D/nM	$\Delta H°$/kcal·mol^{-1}	$T\Delta S°$/kcal·mol^{-1}
RBP[a]	170 ± 9	−11.0 ± 0.1	−1.4 ± 0.1	28.0 ± 4	−11.0 ± 0.2	−0.3 ± 0.05
GGBP[b]	290 ± 20	−21.0 ± 0.3	−11.7 ± 0.4	237 × 10^3 ± 1530	−21 ± 0.5	−15.8 ± 0.6

[a]Affinity for D-ribose. [b]Affinity for D-glucose. [c]Experiment carried out at 310 K.

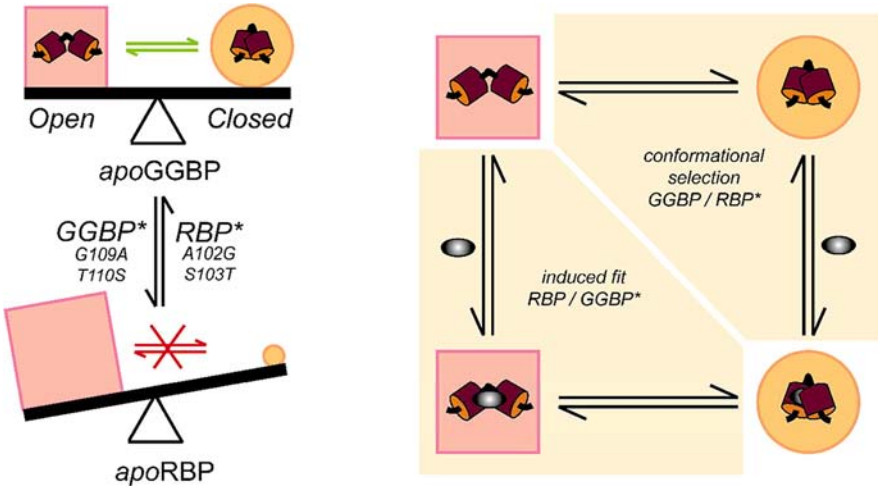

Figure 4. Conformational equilibria for GGBP and RBP. Left: experimental data indicate the coexistence of open and closed conformations for *apo*GGBP, while a single (open) conformation dominates for *apo*RBP. Interconversion between such conformations may (green arrow) or may not (red arrow) be possible, according to the experimental data set. This situation can be reverted upon mutation in the hinge region. Right: conformational rearrangement and ligand binding may proceed through two different mechanisms: induced fit (consistent with data for RBP and GGBP*) and conformational selection (consistent with data for GGBP and RBP*).

mutant proteins, with and without monosaccharide ligand. These data reveal that the hinge dynamics of GGBP* differ decisively from *wt*GGBP and instead become very similar to wt RBP, from which the two point mutations in the hinge region were derived. In particular, the pervasive fast dynamics found in *wt*GGBP is now lost (Figure 3), and the conformational entropy change correspondingly reduces to $\overline{\Delta \mathbf{S}_i} = -0.26 \pm 0.1$ J·mol^{-1}·K^{-1} (Figure S7), very similar to the value obtained for wt RBP. The complementary mutant RBP* conversely adopts the hinge dynamics from *wt*GGBP, the progenitor of its two point mutations in the hinge region: the formerly erratic ΔS^2 changes in order parameters now show the clear net increase found in *wt*GGBP and, correspondingly, a net decrease in conformational entropy $\overline{\Delta \mathbf{S}_i}$ by −2.1 ± 0.3 J·mol^{-1}·K^{-1}, comparable with *wt*GGBP. Thus, the motions indicated by the order parameters S^2 for *glu*GGBP (and for *glu*RBP* with similarly reengineered hinge region) likely represent correlated segment motions that are ultimately controlled by the hinge residue composition.

Functional Dynamics for RBP and GGBP. To check whether the observed dynamics interfere with the PBP function, the natural substrate affinities were measured by isothermal titration calorimetry for wt and mutant proteins (Table 1 and Figure S9). Very high affinities were observed for D-ribose (RBP) and D-glucose (GGBP), in line with previously reported affinity constants measured by other techniques.[51,52] The mode of carbohydrate binding is very similar in both proteins, where the monosaccharide is stabilized by a network of cooperative hydrogen bonds with polar side-chain residues.[10] Except for N256 in GGBP and the equivalent Q235 in RBP, no hinge residue is involved in stabilizing the ligand. As shown in Table 1, however, the two hinge residue mutations drastically alter the apparent sugar binding constant, and GGBP* binds D-glucose with ca. 550-fold *weaker* affinity. Remarkably, RBP* conversely binds D-ribose with 10-fold *stronger* affinity than wt RBP. The thermodynamic parameters extracted from the ITC data reveal that the differences in affinity measured are caused exclusively by changes in the entropy of the system, in full agreement with the NMR relaxation data analysis. As mentioned above, the structural data do not suggest that these mutations modify the protein−carbohydrate interaction network, hypothesis supported by the identical binding enthalpies found (Table 1). Instead, both hinge residue mutations apparently alter the open-to-close transition that is energetically coupled to the intrinsic affinity for the ligand.

DISCUSSION

Despite structural homology,[38] our data suggest different functional mechanisms for the two analyzed PBPs, GGBP, and RBP. For *apo*RBP, a static picture with open interdomain orientation (represented by the solution NMR structure) agrees well with most of the previously reported data[21,28,42,53] and our ^{15}N relaxation data. According to molecular simulations,[42] the closed domain conformation would be almost inaccessible for *apo*RBP due to the large activation barrier separating both states (115 kcal·mol^{-1}) and should at most represent 5% of the population of states (Figure 4). Contrarily, excursions toward a more open state are conceivable since a single mutation suffices to produce a wider open conformation in the crystalline phase.[29] The sporadic nature of such transitions would make them undetectable by NMR relaxation measurements, although RDCs in combination with paramagnetic relaxation enhancement have proven very useful

dx.doi.org/10.1021/ja3092938 | J. Am. Chem. Soc. 2012, 134, 19869−19876

in detecting such small populations in the functionally related maltose binding protein.[18]

In contrast to RBP, a single structural model is incompatible with the vast conformational space covered by *apo*GGBP in solution. Early studies with ^{19}F NMR[54] and disulfide trapping[55] have already suggested the existence of large amplitude motions in *apo*GGBP, in accordance with the multiple hinge angles found in the deposited X-ray structures (Table S1 and Figure 4). Collective motions would have to occur with correlation times between 10^{-4} s and 10^{-8} s since the molecular alignment tensor (derived from RDC data) differs significantly from the rotational diffusion tensor (derived from NMR relaxation data) while order parameters S^2 are not significantly reduced. This is consistent with recent semiatomistic molecular simulations.[56] Upon glucose binding, a general decrease in S^2 is observed that proves such hinge motions persist in *holo*GGBP, however, on a faster nanosecond time scale (≤12 ns). The neat entropic contribution found reflects an increase in dynamics that shall be attributed to coupled motions between the two domains. Obviously, interdomain dynamics in *glu*GGBP can only have small amplitudes to retain the bound ligand. This is consistent with the 9° variation in the closure angle observed among the ligand-bound structures[23] and with the structural analysis of the obtained rotational diffusion tensor. Rather than destabilizing the complex, calorimetric data support the notion that such interdomain motions enhance the apparent affinity (Table 1).

From a functional point of view, the open-to-close transition is thermodynamically coupled with the intrinsic ligand affinity (Figure 4). Two opposite mechanisms can be conceived:[57] (i) the ligand actively reshapes the binding site by interacting with the protein (*induced fit*), or (ii) the closed conformation already exists in the *apo* form with low propensity and gets stabilized by the ligand binding (*conformational selection*). For RBP (with a *single* structure satisfying all experimental data), experiments better agree with an induced fit mechanism, as in the glutamine binding protein.[22] Nevertheless, the existence of a small population of *apo*RBP in a closed conformation, as for maltose binding protein,[18] cannot be ruled out on the basis of the available data. On the other hand, the averaged solution structure of *apo*GGBP reveals a semiclosed conformation that clearly suggests the presence of multiple states and, ultimately, a conformational selection mechanism (Figure 4). Previous observations on *apo*GGBP[23,55] and our ^{15}N relaxation data corroborate this interpretation. The hinge region plays a pivotal role in the open-to-close transition, and only two-point mutations there can alter the interdomain dynamics and, by consequence, relative populations of open and closed conformations.

The large conformational rearrangement associated with the binding-induced closure mechanism in PBPs has been extensively exploited for the design of protein-based biosensors, where a tag for detecting the conformational change (e.g., by fluorescence) is typically attached to the protein.[58] There is a persistent great interest in developing efficient and sensitive methods to monitor glucose levels in patients with diabetes, a severe chronic condition that affects over 100 million people worldwide.[13] Unfortunately, it is impossible to use *wt*GGBP or RBP as sensors since their affinity is far too high for the physiological glucose levels (1.7−33 mM). To reduce their glucose affinity, these PBPs have been reengineered in their binding site[59−61] where mutations, however, entail a high risk of severely degrading the natural ligand specificity. Moreover, the computational design of receptors built in the PBP fold is not a solved problem.[62] Our studies suggest a novel way for reducing the PBP ligand affinity *without* affecting its intrinsic affinity for the ligand, by reengineering the hinge region instead of the active site: only the hinge dynamics and relative populations of open (amenable to ligand binding) and closed (largely blocked for ligand binding) conformations are modulated.

CONCLUSION

In summary, we describe distinctly different binding mechanisms for two structurally related, bacterial periplasmic binding proteins. Interdomain segmental motions are functionally relevant since they alter the apparent affinity for the substrate and are governed by the hinge region amino acid composition.

ASSOCIATED CONTENT

Supporting Information

Nine figures and four tables including NMR spectra of the involved proteins, sequence alignment, and fitted data. This material is available free of charge via the Internet at http://pubs.acs.org.

AUTHOR INFORMATION

Corresponding Author

omillet@cicbiogune.es

Notes

The authors declare no competing financial interest.

ACKNOWLEDGMENTS

We thank Lewis Kay and Ranjith Muhandiram (Univ of Toronto) for the spectrometer time and helpful discussions. Support was provided from The Department of Industry, Tourism and Trade of the Government of the Autonomous Community of the Basque Country, from the Innovation Technology Department of the Bizkaia County, from the Ministerio de Economía y Competititvidad (CTQ2009-10353/BQU, CTQ2012-32183, and CSD2008-00005). G.O. acknowledges a fellowship from the Ministerio de Ciencia y Tecnología.

REFERENCES

(1) Gerstein, M.; Lesk, A. M.; Chothia, C. *Biochemistry* **1994**, *33*, 6739−6749.
(2) Ma, B.; Tsai, C. J.; Haliloglu, T.; Nussinov, R. *Structure* **2011**, *19*, 907−917.
(3) Mittag, T.; Kay, L. E.; Forman-Kay, J. D. *J. Mol. Recognit.* **2010**, *23*, 105−116.
(4) Swain, J. F.; Gierasch, L. M. *Curr. Opin. Struct. Biol.* **2006**, *16*, 102−108.
(5) Gerstein, M.; Krebs, W. *Nucleic Acids Res.* **1998**, *26*, 4280−4290.
(6) Quiocho, F. A.; Ledvina, P. S. *Mol. Microbiol.* **1996**, *20*, 17−25.
(7) Bordignon, E.; Grote, M.; Schneider, E. *Mol. Microbiol.* **2010**, *77*, 1354−1366.
(8) Manson, M. D.; Armitage, J. P.; Hoch, J. A.; Macnab, R. M. *J. Bacteriol.* **1998**, *180*, 1009−1022.
(9) Vyas, N. K.; Vyas, M. N.; Quiocho, F. A. *Proc. Natl. Acad. Sci. U.S.A.* **1983**, *80*, 1792−1796.
(10) Vyas, N. K.; Vyas, M. N.; Quiocho, F. A. *Science* **1988**, *242*, 1290−1295.
(11) Huang, S.; Cao, J.; Jiang, M.; Labesse, G.; Liu, J.; Pin, J. P.; Rondard, P. *Proc. Natl. Acad. Sci. U.S.A.* **2011**, *108*, 15480−15495.
(12) Zhang, F.; Klebansky, B.; Fine, R. M.; Liu, H.; Xu, H.; Servant, G.; Zoller, M.; Tachdjian, C.; Li, X. *Proc. Natl. Acad. Sci. U.S.A.* **2010**, *107*, 4752−4757.
(13) Jeffery, C. J. *Nano Rev* **2011**, *2*, 1−4.

(14) Vercillo, N. C.; Herald, K. J.; Fox, J. M.; Der, B. S.; Dattelbaum, J. D. *Protein Sci.* **2007**, *16*, 362−368.
(15) Loeffler, H. H.; Kitao, A. *Biophys. J.* **2009**, *97*, 2541−2549.
(16) Stockner, T.; Vogel, H. J.; Tieleman, D. P. *Biophys. J.* **2005**, *89*, 3362−3371.
(17) Skrynnikov, N. R.; Goto, N. K.; Yang, D.; Choy, W. Y.; Tolman, J. R.; Mueller, G. A.; Kay, L. E. *J. Mol. Biol.* **2000**, *295*, 1265−1273.
(18) Tang, C.; Schwieters, C. D.; Clore, G. M. *Nature* **2007**, *449*, 1078−1082.
(19) Flocco, M. M.; Mowbray, S. L. *J. Biol. Chem.* **1994**, *269*, 8931−8936.
(20) Millet, O.; Hudson, R. P.; Kay, L. E. *Proc. Natl. Acad. Sci. U.S.A.* **2003**, *100*, 12700−12705.
(21) Shilton, B. H.; Flocco, M. M.; Nilsson, M.; Mowbray, S. L. *J. Mol. Biol.* **1996**, *264*, 350−363.
(22) Bermejo, G. A.; Strub, M. P.; Ho, C.; Tjandra, N. *Biochemistry* **2010**, *49*, 1893−1902.
(23) Borrok, M. J.; Kiessling, L. L.; Forest, K. T. *Protein Sci.* **2007**, *16*, 1032−1041.
(24) Delaglio, F.; Grzesiek, S.; Vuister, G. W.; Zhu, G.; Pfeifer, J.; Bax, A. *J. Biomol. NMR* **1995**, *6*, 277−293.
(25) Castano, D.; Millet, O. *Biomol. NMR Assign.* **2011**, *5*, 31−34.
(26) Kontaxis, G.; Clore, G. M.; Bax, A. *J. Magn. Reson.* **2000**, *143*, 184−196.
(27) Evenas, J.; Tugarinov, V.; Skrynnikov, N. R.; Goto, N. K.; Muhandiram, R.; Kay, L. E. *J. Mol. Biol.* **2001**, *309*, 961−974.
(28) Cuneo, M. J.; Beese, L. S.; Hellinga, H. W. *BMC Struct. Biol.* **2008**, *8*, 50.
(29) Bjorkman, A. J.; Mowbray, S. L. *J. Mol. Biol.* **1998**, *279*, 651−664.
(30) Bjorkman, A. J.; Binnie, R. A.; Zhang, H.; Cole, L. B.; Hermodson, M. A.; Mowbray, S. L. *J. Biol. Chem.* **1994**, *269*, 30206−30211.
(31) Brunger, A. T.; Adams, P. D.; Clore, G. M.; DeLano, W. L.; Gros, P.; Grosse-Kunstleve, R. W.; Jiang, J. S.; Kuszewski, J.; Nilges, M.; Pannu, N. S.; Read, R. J.; Rice, L. M.; Simonson, T.; Warren, G. L. *Acta Crystallogr. D: Biol. Crystallogr.* **1998**, *54*, 905−921.
(32) Farrow, N. A.; Muhandiram, R.; Singer, A. U.; Pascal, S. M.; Kay, C. M.; Gish, G.; Shoelson, S. E.; Pawson, T.; Forman-Kay, J. D.; Kay, L. E. *Biochemistry* **1994**, *33*, 5984−6003.
(33) Bruschweiler, R.; Liao, X.; Wright, P. E. *Science* **1995**, *268*, 886−889.
(34) Lee, L. K.; Rance, M.; Chazin, W. J.; Palmer, A. G., III *J. Biomol. NMR* **1997**, *9*, 287−298.
(35) Lipari, G.; Szabo, A. *J. Am. Chem. Soc.* **1982**, *104*, 4546−4559.
(36) Skrynnikov, N. R.; Millet, O.; Kay, L. E. *J. Am. Chem. Soc.* **2002**, *124*, 6449−6460.
(37) Yang, D.; Kay, L. E. *J. Mol. Biol.* **1996**, *263*, 369−382.
(38) Vyas, N. K.; Vyas, M. N.; Quiocho, F. A. *J. Biol. Chem.* **1991**, *266*, 5226−5237.
(39) Vyas, N. K.; Vyas, M. N.; Quiocho, F. A. *Nature* **1987**, *327*, 635−638.
(40) Zukin, R. S.; Strange, P. G.; Heavey, R.; Koshland, D. E. *Biochemistry* **1977**, *16*, 381−386.
(41) Tjandra, N.; Bax, A. *Science* **1997**, *278*, 1111−1114.
(42) Ravindranathan, K. P.; Gallicchio, E.; Levy, R. M. *J. Mol. Biol.* **2005**, *353*, 196−210.
(43) Palmer, A. G., III *Annu. Rev. Biophys. Biomol. Struct.* **2001**, *30*, 129−155.
(44) Zheng, Z.; Czaplicki, J.; Jardetzky, O. *Biochemistry* **1995**, *34*, 5212−5223.
(45) Arumugam, S.; Gao, G.; Patton, B. L.; Semenchenko, V.; Brew, K.; Van Doren, S. R. *J. Mol. Biol.* **2003**, *327*, 719−734.
(46) Yun, S.; Jang, D. S.; Kim, D. H.; Choi, K. Y.; Lee, H. C. *Biochemistry* **2001**, *40*, 3967−3973.
(47) Akke, M. *Biochem. Soc. Trans.* **2012**, *40*, 419−423.
(48) MacRaild, C. A.; Daranas, A. H.; Bronowska, A.; Homans, S. W. *J. Mol. Biol.* **2007**, *368*, 822−832.
(49) Clore, G. M.; Szabo, A.; Bax, A.; Kay, L. E.; Driscoll, P. C.; Gronenborn, A. M. *J. Am. Chem. Soc.* **1990**, *112*, 4989−4991.
(50) Yang, D.; Mok, Y. K.; Forman-Kay, J. D.; Farrow, N. A.; Kay, L. E. *J. Mol. Biol.* **1997**, *272*, 790−804.
(51) Aqvist, J.; Mowbray, S. L. *J. Biol. Chem.* **1995**, *270*, 9978−9981.
(52) Binnie, R. A.; Zhang, H.; Mowbray, S.; Hermodson, M. A. *Protein Sci.* **1992**, *1*, 1642−1651.
(53) Cuneo, M. J.; Tian, Y.; Allert, M.; Hellinga, H. W. *BMC Struct. Biol.* **2008**, *8*, 20.
(54) Luck, L. A.; Falke, J. J. *Biochemistry* **1991**, *30*, 6484−6490.
(55) Careaga, C. L.; Sutherland, J.; Sabeti, J.; Falke, J. J. *Biochemistry* **1995**, *34*, 3048−3055.
(56) Cashman, D. J.; Mamonov, A. B.; Bhatt, D.; Zuckerman, D. M. *Curr. Top. Med. Chem.* **2011**, *11*, 211−220.
(57) Bucher, D.; Grant, B. J.; Markwick, P. R.; McCammon, J. A. *PLoS Comput. Biol.* **2011**, *7*, e1002034.
(58) Dwyer, M. A.; Hellinga, H. W. *Curr. Opin. Struct. Biol.* **2004**, *14*, 495−504.
(59) Der, B. S.; Dattelbaum, J. D. *Anal. Biochem.* **2008**, *375*, 132−140.
(60) Khan, F.; Saxl, T. E.; Pickup, J. C. *Anal. Biochem.* **2010**, *399*, 39−43.
(61) Sakaguchi-Mikami, A.; Taneoka, A.; Yamoto, R.; Ferri, S.; Sode, K. *Biotechnol. Lett.* **2008**, *30*, 1453−1460.
(62) Schreier, B.; Stumpp, C.; Wiesner, S.; Hocker, B. *Proc. Natl. Acad. Sci. U.S.A.* **2009**, *106*, 18491−18496.